# DETECTION OF SUBSURFACE MATERIAL SEPARATION IN SHUTTLE ORBITER SLIP-SIDE JOGGLE REGION OF THE WING LEADING EDGE USING INFRARED IMAGING DATA FROM ARC-JET TESTS

Kamran Daryabeigi and Sandra P. Walker
NASA Langley Research Center
Hampton, VA 23681

## ABSTRACT

The objective of the present study was to determine whether infrared imaging (IR) surface temperature data obtained during arc-jet tests of Space Shuttle Orbiter's reinforced carbon-carbon (RCC) wing leading edge panel slip-side joggle region could be used to detect presence of subsurface material separation, and if so, to determine when separation occurs during the simulated entry profile. Recent thermostructural studies have indicated thermally induced interlaminar normal stress concentrations at the substrate/coating interface in the curved joggle region can result in local subsurface material separation, with the separation predicted to occur during approach to peak heating during reentry. The present study was an attempt to determine experimentally when subsurface material separations occur.

A simplified thermal model of a flat RCC panel with subsurface material separation was developed and used to infer general surface temperature trends due to the presence of subsurface material separation. IR data from previously conducted arc-jet tests on three test specimens were analyzed: one without subsurface material separation either pre or post test, one with pre test separation, and one with separation developing during test. The simplified thermal model trend predictions along with comparison of experimental IR data of the three test specimens were used to successfully infer material separation from the arc-jet test data. Furthermore, for the test specimen that had developed subsurface material separation during the arc-jet tests, the initiation of separation appeared to occur during the ramp up to the peak heating condition, where test specimen temperature went from 2500 to 2800°F.

## NOMENCLATURE

| | |
|---|---|
| L | length of test specimen (streamwise/chordwise direction) |
| T | temperature |
| t | time |
| W | width of test specimen (spanwise direction) |
| x | spanwise coordinate |
| y | streamwise coordinate |
| $\delta T$ | difference in surface temperature prediction for model with and without subsurface material separation |
| $\Delta T$ | difference in experimental surface temperature of joggle region and region immediately downstream of joggle |

## INTRODUCTION

Two reinforced carbon-carbon (RCC) wing leading edge panels on the Space Shuttle Orbiter have experienced spallation of their silicon-carbide (SiC) coating. The loss of coating during the heating portion of reentry could possibly lead to a catastrophic burn through in the RCC substrate. A photograph of an Orbiter panel that had experienced coating liberation is shown in

---

* Distribution Statement A: Approved for public release; distribution is unlimited

Figure 1 along with a schematic illustrating the general arrangement of panels and T-seals. The T-seals, located between adjacent panels, are designed to prevent flow ingress during entry while allowing free thermal expansion of the panels across the span of the wing. The coating spallations had occurred on the slip-side joggle region of the panels.

Due to the risk associated with loss of coating during flight, an investigation had been initiated to determine the root cause for the coating spallation. Nondestructive evaluation (NDE) techniques had revealed subsurface defects in the slip-side joggle region of several panels. Subsequent microscopic analysis of select panels with NDE anomalies had revealed subsurface material separation in the joggle, contained mostly in the RCC substrate material near the outer-mold-line (OML) SiC coating interface (Ref. 1). A study utilizing thermostructural analysis of the slip-side joggle region was initiated to determine the root cause for the initiation of the material separations (Ref. 2). The results of this study (Ref. 2) revealed that thermally induced interlaminar normal stress concentrations in the substrate/coating interface in the curved joggle region can result in local subsurface material separation, and that this separation occurs during approach to peak heating condition during reentry. Furthermore, during arc-jet testing of local joggle/ T-seal specimens one of the specimens tested experienced joggle subsurface material separation during the test (Ref. 3).

The objective of the present study was to analyze IR imaging surface temperature data previously obtained during the arc-jet tests in order to determine whether subsurface material separation (SMS) locations could be identified during the arc-jet tests, and if so, to determine the separation initiation time. IR imaging surface temperature data had previously been used to infer aero-heating rates from hypersonic wind tunnel tests (Ref. 4) and arc-jet tests (Ref. 5), but have never been utilized to infer subsurface properties/defects such as material separation from wind tunnel or arc-jet tests. A simplified thermal model of a flat RCC panel with SMS was developed and used to infer general surface temperature trends due to the presence of material separation. IR data from three arc-jet test specimens were analyzed: one without material separation either pre or post test, one with pre-test separation, and one with separation developing during test. The comparison of IR surface temperature measurements in the joggle region of the three test specimens along with the simplified thermal model trends were used to determine SMS locations and the initiation time of separation.

## ARC-JET TESTS

Arc-jet tests had previously been conducted in the NASA Johnson Space Center (JSC) Atmospheric Reentry Materials and Structures Evaluation Facility (ARMSEF) on a wedge model holder (Ref. 3). A photograph of the test specimen in the water-cooled copper wedge model holder is shown in Figure 2a. The overall test specimen length and width were 4.875 and 4.375 inch, respectively, and consisted of the T-seal and an adjacent panel section with a joggle. The slip-side joggle region is located at the edge of the panel section adjacent to the T-seal, with a gap between the joggle and T-seal sections as shown in the figure. A representative IR image of the test specimen obtained during the tests is shown in Figure 2b. The geometrical notation used in analysis of IR data is also overlaid on the IR image. A close-up photograph of the cross-sectional area of the test article in the vicinity of the slip-side joggle is shown in Figure 3.

IR imagery data had been obtained using a near IR imager with spectral response of 0.8 to 0.9 micrometers. The IR system generates 30 frames per second, but data for the tests reported here had been stored at a rate of 4 frames per second. The IR surface temperature data had been obtained using a constant emittance value of 0.9 for the SiC-coated RCC panel. The random noise of the IR data analyzed in this study varied between 10 and 40°F depending on the temperature range and span setting of the imaging system during the tests. The IR surface temperature measurements were generally higher than temperatures measured using two optical pyrometers used for monitoring surface temperatures on the T-seal and panel sections, but this

did not have any relevance to the data analysis presented here, since relative change in temperatures instead of absolute temperatures was required for this analysis.

A typical optical pyrometer surface temperature measurement obtained during these arc-jet tests is shown in Figure 4. The arc-jet temperature profile consisted of 6 steps summarized in Table 1. The temperatures provided in the table are nominal test condition values, and measured surface temperatures shown in the figure are slightly different. The time associated with test article becoming stationary at the test section centerline (arc flow is established first, then the model is injected into the test section) was designated as zero second. Steps 1 through 3 consisted of three distinct temperature ramp ups and dwells at various temperatures. Step 1 consisted of typical ramp up and dwell at 2000°F starting at 200 sec, step 2 consisted of ramp up and dwell at 2500°F starting at 260 sec, while step 3 consisted of ramp up and dwell at 2800°F starting at 370 sec. The dwell time at 2800°F during step 3 typically lasted 670 sec. Steps 4 through 6 consisted of three distinct temperature ramp downs and dwells at various temperatures. Step 4 consisted of typical ramp down and dwell at 2500°F starting at 1060 sec, step 5 consisted of ramp down and dwell at 2000°F starting at 1200 sec, while step 6 consisted of ramp down starting at 1400 sec achieved by turning the arc off.

IR data from three arc-jet test specimens, listed in Table 2**,** were analyzed in this study. Test specimen 2638 had no significant SMS either pre or post arc-jet test based on NDE results. Test specimen 2637 had no SMS prior to arc-jet test, and developed significant material separation in the joggle region during the arc-jet test. The post-test NDE normalized indications for this test specimen varied between 0.2 and 0.6 across the whole width of the joggle region. Orbiter panels with NDE normalized amplitude of 0.2 or higher are considered for replacement. Test specimen 2641 NDE normalized indications varied between 0.2 and 0.3 across the whole width of the joggle region before the test, and increased to between 0.3 and 0.5 after its first cycle arc-jet test. The comparison of arc-jet IR surface temperature data in the joggle region of test specimen 2637 (which developed SMS during the test) with test specimens with no SMS (test specimen 2638) and pre-existing SMS (test specimen 2641) was used as a guide to investigate whether SMS signature could be detected.

## SIMPLIFIED THERMAL MODEL

First, a one-dimensional (through thickness) finite volume thermal model of the arc-jet test specimen was developed to infer imposed transient heat fluxes on the model from the optical pyrometer surface temperature measurements on the T-seal region (upstream of the joggle) shown in Figure 4. Even though the heat flux actually varies across the length of the test specimen in arc-jet testing, for simplicity it was assumed that the inferred heat fluxes were invariant across the test specimen at any instant of time. Then, a two-dimensional finite volume thermal model of a flat RCC panel was developed to represent heat transfer in both the streamwise and through-thickness directions. The simplified geometry considered is shown in Figure 5, and consisted of a 4-inch long, 0.15-inch thick flat RCC section, covered by 0.04-inch thick SiC coating on either side. Subsurface material separation was modeled as 0.25-inch long, 0.005-inch thick gap at the OML coating/RCC interface located halfway across the length of the panel. Even though the actual arc-jet test specimen has a complicated geometry and the joggle region is highly curved, the intent of this thermal modeling was not to model the exact geometry, but to infer general trends due to subsurface material separation from a very simple geometrical model. These trends were then subsequently used as guides for interpreting the arc-jet IR surface temperatures for the various test specimens. Separation region was thermally approximated as a contact resistance between the coating and RCC, with the contact resistance calculated assuming that heat transfer in the gap consisted of radiation and gas conduction between two parallel plates with a 0.005-inch gap thickness. Therefore, the geometry of the model was not changed due to material separation and only a contact resistance term was added to the thermal model.

The transient surface heat fluxes inferred from the one-dimensional finite volume model were applied on the OML of the two-dimensional flat RCC panel geometry, assuming no spatial variation in heat flux. Adiabatic boundary conditions were applied on the back (IML) and the sides of the thermal model. Efficient high-temperature insulation was utilized on the backside of the RCC arc-jet test specimen in the wedge model to minimize heat losses between RCC panel and the water-cooled copper wedge model holder, so the assumption of adiabatic backface boundary condition is justified. A linearly varying temperature distribution through the thickness of the entire model with the OML at 1400°F and IML at 150°F was used as the initial condition. This accounted for heating of the test article during the model injection process, from when it crosses the jet flow edge until it becomes stationary at test section centerline (t = 0 sec). An alternating direction implicit (ADI) method (Ref. 6) was used to solve the transient two-dimensional heat conduction problem.

Temperature solutions for the simplified RCC model were obtained both with and without simulated SMS. The difference between predicted transient surface temperatures on top of the separated region for models with and without separation is shown in Figure 6. Separation signature ($\delta$T), difference between surface temperatures for separated and non-separated subsurface, is detectable during the transient portion of each step (ramp up or down), and manifests itself as locally warmer region (above the separation region) during the temperature ramp up steps (steps 1 through 3), and locally cooler region during the temperature ramp down steps (steps 4 through 6). Separation signature disappears during the dwell portion of each step due to high lateral thermal conductivity of both SiC coating and RCC. Magnitude of separation signature is highest in step 6 (ramp down with arc off) and lowest in step 4 (ramp down to 2500°F).

Variation of separation signature magnitude with occurrence time of SMS during an arc-jet test step was investigated for the specific case of arc-jet step 3. This step extends from 370 to 1060 sec, with the ramp up portion of the step occurring over the 370-400 sec interval. Separation signatures caused by subsurface material separation occurring at 371, 385 and 390 sec are shown in Figures 7a, 7b, and 7c, respectively. For separation occurring at 371 sec, the maximum $\delta$T is 38°F and occurs at 381 sec. A close-up of this separation signature is shown in Figure 8. Separation signature develops around 371 seconds, and its magnitude rises till 381 sec, and then drops and becomes undetectable after approximately 398 sec. The magnitude of this separation signature is similar to pre-existing separation. For separation occurrence at 385 and 390 sec, the maximum separation signatures are 27°F and 15°F, occurring at 388 and 393 seconds, respectively. Therefore, the magnitude of $\delta$T during the step decreases as separation occurrence time shifts towards the end of the ramp section of that step, and separation occurrence time in one step does not affect separation signature in the following steps. Also, there is a certain time delay between occurrence of separation and time when separation signature is at its maximum and more easily detectable. Separations occurring at 400 and 750 sec do not have any detectable separation signatures during Step 3. So, if separation happens towards the end of the temperature ramp ups or downs, its signature will be very low and may not be detectable during that step. Also, separation occurring during the dwell portion of each step (constant temperature portion of step) can not be detected until the following ramp up or down step.

The predicted transient surface temperatures during step 2 of arc-jet test for model with no separation and model with separation prior to step 2 are shown in Figure 9. Figure 10 shows predicted transient surface temperatures during step 3 of arc-jet test for when separation occurs during the step, in this case separation occurring at 385 sec. These transient surface temperature trends will be used for determining whether an observed separation signature during the arc-jet steps had occurred either prior to or during the step.

## RESULTS AND DISCUSSION

The streamwise distribution of IR surface temperature data at mid-span (x/W = 0.5) at a specific time within the ramp up or down portion of each step for the three test specimens were compared. Figure 11 shows a typical IR image of one of the test specimens (test specimen 2641 during step 6) with the associated streamwise temperature distribution. All the streamwise temperature distributions presented here were subjected to a Blackman noise reduction filter (Ref. 7) to remove some of the random noise. The gap between the T-seal and joggle region on the panel appears to be cooler than the surrounding regions during the heating steps (steps 1 through 3), and warmer during the cooling steps (steps 4 through 6). These effects result from the interior regions surrounding the gap remaining cooler than the OML surfaces directly exposed to flow during the heating steps, and not cooling off as fast as OML surfaces during the cooling steps. The gap location for each model is designated as zero streamwise location (y/L = 0). The variation of surface temperature data at the joggle region, region immediately downstream of gap and marked in the line drawing in Figure 11, was compared to temperatures both downstream and upstream of the joggle (on the T-seal) for each test specimen. The comparison of the spatial temperature distributions in the joggle region of the three test specimens in conjunction with expected trends from the simplified thermal model were used to determine subsurface material separation. Referring to Figure 11, the temperatures in the joggle region, marked as SMS in figure, is 73°F ($\Delta$T) cooler than the immediate region downstream of joggle, and is different from temperatures immediately upstream of the joggle on the T-seal. The cooler region in the joggle area was 0.26-inch wide. This joggle region was designated as having had subsurface material separation, consistent with NDE results. Joggle region was designated as having had SMS if it met the following criteria:

- It had a significantly wide (0.15 inch or more) region with temperature difference ($\Delta$T) of at least 10°F compared to adjoining region downstream of joggle.
- Temperature at the joggle region was different from temperature immediately upstream of joggle on the T-seal.

These criteria were established after detailed analysis of arc-jet data from the three test specimens. For any joggle region determined to have had SMS, the following information will be provided: approximate width of separation zone, and approximate temperature difference ($\Delta$T) between joggle and immediate region downstream of joggle.

A few complications associated with the IR imagery data should be mentioned. The IR images of the various test specimens did not line up, mainly because different test specimens were located at slightly different streamwise locations in the test section for the various tests. Test specimen 2641 was farthest away from the nozzle, therefore had lower surface temperatures compared to the other two specimens. The surface temperature variations between the test specimens could also have possibly been caused by variations in arc-jet test conditions. Also, the test specimens moved upstream with respect to the nozzle by approximately 0.3-inch during each test due to thermal expansion of model support. To compensate for these complications, the center of gap location between T-seal and panel sections for each test article at various times during the test was designated as zero streamwise location (y/L = 0). Another complication with determination of subsurface material separation location was using the criterion of temperature difference of at least 10°F between joggle and adjoining downstream region when the random noise of IR surface temperature data varied between 10 and 40°F. As previously stated, the streamwise temperature distributions presented here were subjected to a noise reduction filter to remove some of the random noise

First the data during the cooling steps will be discussed in reverse chronological order. The subsurface material separation signature in these steps is typically stronger, and determination of

separation regions more straight forward. Then, data during the heating steps will be discussed in chronological order.

The IR images of the three test specimens during step 6 of arc-jet test at approximately 1406 sec (6 sec after initiation of step 6) are provided in Figure 12. For all the IR images presented in this discussion, the IR image of test specimen 2638 (without either pre or post test SMS) is shown on the left, while the IR image of the test specimen 2641 (with both pre and post test SMS) is shown on the right. The IR image of test specimen 2637 (developed SMS during the test) is shown in the middle. The gap between the joggle and T-seal regions appears warmer than the surrounding regions during all the cooling steps as discussed previously. Comparison of IR surface temperatures images in the joggle region of the three test specimens at 1406 sec indicated that both test specimens 2637 and 2641 had a distinctly cooler region in the joggle region compared to both downstream and upstream regions of the joggle. This observation was in accordance with the simplified thermal model prediction that region with SMS would exhibit locally cooler surface temperatures during the ramp down section of cooling steps. This behavior was not evident for test specimen 2638. Comparison of streamwise temperature distributions at mid-span (x/W = 0.5) for the three test specimens is shown in Figure 13. Test specimen 2641 joggle had a 0.26-inch wide region that had a maximum temperature difference ($\Delta$T) of 73°F compared to the region immediately downstream of joggle, and its temperature was different from the T-seal region immediately upstream of the gap. Test specimen 2637 joggle had a 0.21-inch wide region with a maximum temperature difference of 38°F compared to the region immediately downstream of joggle, and its temperature was different from the T-seal region immediately upstream of the gap. This behavior was not observed for test specimen 2638. Therefore, the joggle regions at mid- span for test specimens 2641 and 2637 were designated as regions with subsurface material separation. These results were in agreement with post-test NDE results.

The IR images of the three test specimens during step 5 of arc-jet test at approximately 1214 sec (14 sec after initiation of step 5) are provided in Figure 14. Both test specimens 2637 and 2641 again had a distinctly cooler region in the joggle region compared to both downstream and upstream regions of the joggle. This behavior was not evident for test specimen 2638. Comparison of streamwise temperature distributions at mid-span (x/W = 0.5) for the three test specimens is shown in Figure 15. Test specimen 2641 joggle had a 0.23-inch wide region with a maximum temperature difference of 17°F compared to the region immediately downstream of joggle, and its temperature was different from the T-seal region immediately upstream of the gap. Test specimen 2637 joggle had a 0.15-inch wide region with a maximum temperature difference of 10°F compared to the region immediately downstream of joggle, and its temperature was different from the T-seal region immediately upstream of the gap. This behavior was not observed for test specimen 2638. The joggle regions at mid-span for test specimens 2641 and 2637 were designated as regions with SMS. The separation signature for step 5 was not as strong as for step 6, consistent with simplified thermal model prediction that highest sensitivity for SMS detection was in step 6.

The IR images of the three test specimens during step 4 of arc-jet test at approximately 1072 sec (12 sec after initiation of step 4) are provided in Figure 16. No distinctly cooler region in the joggle region could be observed for any of the test specimens. Comparison of streamwise temperature distributions at mid-span (x/W = 0.5) for the three models is shown in Figure 17. No distinctly cooler region in the joggle region can be observed for any of the test specimens, therefore, it was concluded that this step had minimal sensitivity for subsurface material separation detection. The simplified thermal model results had also predicted that this step would have the lowest sensitivity to SMS detection.

At this point it was concluded that the IR surface temperature data from arc-jet tests could be used for detecting subsurface material separation. The pre-existing SMS for test specimen 2641 was detected in steps 5 and 6. The SMS that had developed during arc-jet testing of test specimen 2637 was also detected during steps 5 and 6 of the arc-jet test. The main question at this point was whether the initiation time of subsurface material separation for test specimen 2637

could be detected. It may have occurred during step 4 of the arc-jet test, but there was low sensitivity to SMS detection in this step, or could have occurred during one of the earlier heating steps. The data from the heating steps (steps 1 through 3) were considered next.

The IR images of the three test specimens during step 1 of arc-jet test at approximately 210 sec (10 sec after initiation of step 1) are provided in Figure 18. The gap between the joggle and T-seal regions appears cooler than the surrounding regions during all the heating steps as discussed previously. Comparison of IR surface temperatures images in the joggle region of the three test specimens at 210 sec indicated that test specimen 2641 had a distinctly warmer region in the joggle region compared to both downstream and upstream regions of the joggle. This observation was in accordance with simplified thermal model prediction that regions with SMS would exhibit locally warmer surface temperatures during the ramp up section of heating steps. This behavior was not evident for test specimens 2638 and 2637. Comparison of streamwise temperature distributions at mid-span (x/W = 0.5) for the three test specimens is shown in Figure 19. Test specimen 2641 joggle had a 0.26-inch wide region with a maximum temperature difference of 37°F compared to the region immediately downstream of joggle, and its temperature was different from the T-seal region immediately upstream of the gap. The joggle regions for test specimens 2637 and 2638 had very narrow regions with distinct temperature peaks compared to regions immediately downstream of joggle and the T-seal region immediately upstream of the gap. This region with the observed temperature peak was too narrow to be subsurface material separation. Therefore, it was concluded that test specimens 2637 and 2638 did not have subsurface material separation during arc-jet step 1. The narrow temperature peaks on the joggle at the edge of the panels may possibly be due to either local heating augmentation on the joggle due to the step and gap condition with the adjacent T-seal, or reflection of the arc.

The IR images of the three test specimens during step 2 of arc-jet test at approximately 270 sec (10 sec after initiation of step 2) are provided in Figure 20. Test specimen 2641 had a distinctly warmer region in the joggle region compared to both downstream and upstream regions of the joggle. This behavior was not evident for test specimens 2638 and 2637. Comparison of streamwise temperature distributions at mid-span (x/W = 0.5) for the three test specimens is shown in Figure 21. Test specimen 2641 joggle had a 0.26-inch wide region with a maximum temperature difference of 84°F compared to the region immediately downstream of joggle, and its temperature was different from the T-seal region immediately upstream of the gap. Test specimen 2637 joggle had a very narrow region with a distinct temperature difference compared to the region immediately downstream of joggle, but its temperature was not different from the T-seal region immediately upstream of the gap. This region on test specimen 2637 could not be labeled as a region with subsurface material separation. No separation signature could be observed for test specimen 2638. The transient surface temperatures averaged over a 0.06-inch long region centered 0.09-inch downstream of the gap (at y/L = 0.018) at mid-span (x/W = 0.5) for test specimens 2637 and 2638 during step 2 are shown in Figure 22. The transient surface temperatures for identical locations on the two models were identical. When compared with thermal model predictions, it can be concluded that for test specimen 2637 there was no SMS prior to step 2 (similar to Figure 9), and no SMS occurred during the ramp up portion of step 2 (similar to Figure 10). For test specimen 2637 no subsurface material separation was observed during arc-jet steps 1 and 2, while separation was observed during steps 5 and 6. Therefore, subsurface material separation must have occurred during either steps 3 or 4, or during the dwell time of step 2. But, as previously discussed, sensitivity to SMS detection in step 4 was very low. The data for arc-jet step 3 were analyzed next in order to determine whether SMS signature could be detected during this step.

The IR images of the three test specimens during step 3 of arc-jet test at approximately 381 sec (11 sec after initiation of step 3) are provided in Figure 23. Test specimen 2641 had a distinctly warmer region in the joggle region compared to both downstream and upstream regions of the joggle. Comparison of streamwise temperature distributions at mid-span (x/W = 0.5) for the three test specimens at 381 sec is shown in Figure 24. Test specimen 2641 joggle had a 0.18-inch wide region with a maximum temperature difference of 93°F compared to the region

immediately downstream of joggle, and its temperature was different from the T-seal region immediately upstream of the gap. Test specimen 2638 also had a temperature peak at the joggle, but its joggle region temperature peak was not different from the T-seal region immediately upstream of the gap, therefore, could not be classified as a subsurface material separation region. Test specimen 2637 joggle had a 0.21-inch wide region with a maximum temperature difference of 19°F compared to the region immediately downstream of joggle, and its temperature was different from the T-seal region immediately upstream of the gap. Therefore, the joggle region on test specimen 2637 during arc-jet step 3 could be classified as a region with subsurface material separation. The transient surface temperatures averaged over a 0.06-inch long region centered 0.09-inch downstream of the gap (at y/L = 0.018) at mid-span (x/W = 0.5) for test specimens 2637 and 2638 during step 3 are shown in Figure 25. The transient surface temperatures for test specimen 2637 rose faster than data for test specimen 2638 from 374 to 383 sec, with a distinct temperature peak between 377 and 382 sec, which is typical indication of subsurface material separation occurring during the step. This temperature peak resembled the simplified thermal model prediction of subsurface material separation pattern occurring during the ramp up portion of heating step shown in Figure 10. There were other reported anomalies during this step of arc-jet tests for this test specimen: significantly higher temperatures downstream of joggle during this step compared to tests on other test specimens, which may have been caused by outgassing during this step. Despite the reported anomalies, the spatial temperature distributions shown in Figure 24, and temporal variation of temperatures shown in Figure 25, demonstrated that for test specimen 2637 subsurface material separation must have occurred between 374 and 383 sec in step 3 of arc-jet test, during the ramp up to the peak heating condition, where test specimen temperature went from 2500 to 2800°F. This result was consistent with thermostructural prediction that separation due to thermally induced interlaminar normal stress concentrations at the substrate/coating interface in the curved joggle region occurs during approach to peak heating during reentry (Ref. 2).

## CONCLUDING REMARKS

Arc-jet tests of Space Shuttle Orbiter's RCC wing leading edge panel slip-side joggle region were analyzed in order to determine whether IR surface temperature data obtained during the tests could be used to detect presence of subsurface material separation, and if so, to determine when separation occurs during the simulated entry profile.

A simplified thermal model of a flat RCC panel with subsurface material separation was developed and used to infer general surface temperature trends due to the presence of subsurface material separation. IR data from arc-jet tests on three test specimens were analyzed: one without subsurface material separation either pre or post test, one with pre-existing separation, and one with separation developing during the test. The simplified thermal model trend predictions along with comparison of experimental IR data of the three test specimens were used to successfully infer subsurface material separation from surface temperature patterns. Furthermore, for the test specimen that developed subsurface material separation during the arc-jet tests, the initiation time of separation could be determined: material separation appeared to occur during the ramp up to the peak heating condition, where specimen temperature went from 2500 to 2800°F. This result was consistent with thermostructural prediction that separation due to thermally induced interlaminar normal stress concentrations at the substrate/coating interface in the curved joggle region occurs during approach to peak heating during reentry (Ref. 2).

## ACKNOWLEDGEMENTS

The authors would like to express their gratitude to the following individuals:

- Justin H. Kerr, NASA JSC, and Clint H. Cragg and Stephen J. Scotti, NASA LaRC, for supporting this study
- Alvaro C. Rodriguez and Ronald K. Lewis, NASA JSC, for their invaluable support with arc-jet test data, especially the IR imaging data

## REFERENCES


1. Opila, E. J., McCue, T. R., and Buehler, J. A., "Microscopy of the Orbiter Wing Leading Edge Reinforced Carbon-Carbon Coating Defects in the Slip Side Joggle Region", NASA TM (to be published)

2. Walker, S. P., and Warren, J., "Thermostructural Analysis of Joggle Region on the Shuttle Orbiter's Reinforced Carbon-Carbon Wing Leading Edge," JANNAF Airbreathing Propulsion Subcommittee Technical Session on Materials and Structures for AirFrame and Propulsion Systems, Cocoa Beach, FL, January 26-29, 2009.

3. Lewis, R. K. and Rodriguez, A. C., "Panel 10L and 6L Slip Side Joggle Arc Jet Tests", NASA Thermal Design Branch Report, JSC- Report (to be published).

4. Daryabeigi, K., Berry, S. A., Horvath, T. J., and Nowak, R. J., "Finite Volume Numerical Methods for Aeroheating Rate Calculations From Infrared Thermographic Data," Journal of *Spacecraft and Rockets*, Vol. 43, No. 1, 2006, pp. 54-62

5. Driver, D. M., Hui, F., Gokcen, T., Raiche, G. A., Balboni, J., Terrazas-Salinas, I, Mayeuax, B., Riccio, J. R., Lin, F., and Lester, D., "Aeroheating Testing Approach for Shuttle Wing Leading Edge Repair Concepts," - *25th AIAA Aerodynamic Measurement Technology and Ground Testing Conference*, v 1, *Collection of Technical Papers - 25th AIAA Aerodynamic Measurement Technology and Ground Testing Conference*, 2006, p 584-594

6. Anderson, D. A., Tannehill, J. C., Pletcher, R. H., *Computational Fluid Mechanics and Heat Transfer*, McGraw-Hill, New York, 1984, pp.117-118.

7. Smith, S. A., *Digital Signal Processing, A Practical Guide for Engineers and Scientists*, Elsevier Science, Burlington, MA, 2003.


Table 1. Typical arc-jet testing steps for RCC joggle tests.

| Step No. | Starting time, sec | Event |
|---|---|---|
| | 0 | Model on centerline |
| 1 | 200 | Ramp up and hold at 2000°F |
| 2 | 260 | Ramp up and hold at 2500°F |
| 3 | 370 | Ramp up and hold at 2800°F |
| 4 | 1060 | Ramp down and hold at 2500°F |
| 5 | 1200 | Ramp down and hold at 2000°F |
| 6 | 1400 | Ramp down, arc turned off |

Table 2. Listing of arc-jet test specimens and their subsurface material separation (SMS) NDE indications (normalized indication of 0.2 or higher represents significant SMS).

| Test Specimen No. | SMS Status | NDE Normalized Indications | |
|---|---|---|---|
| | | Pre test | Post test |
| 2638 | No SMS pre or post test | ≤ 0.02 | ≤ 0.02 |
| 2637 | SMS during test | ≤ 0.02 | 0.2 – 0.6 |
| 2641 | SMS prior to test | 0.2 – 0.3 | 0.3 – 0.5 |

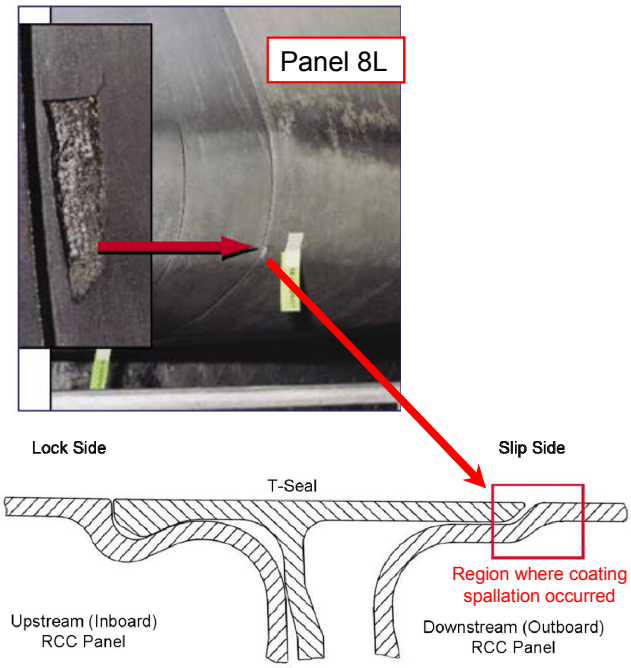


Figure 1. Photograph of Orbiter Panel 8L which had experienced coating spallation and schematic illustrating panel arrangements and where coating spallation had occurred.

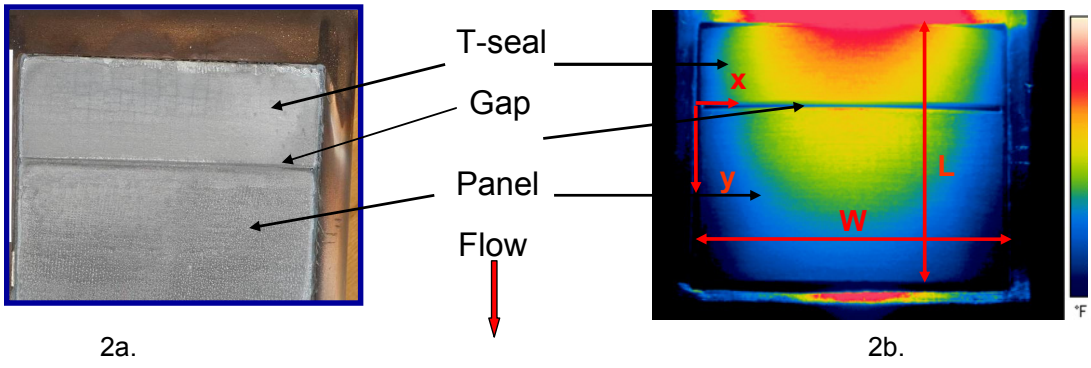


Figure 2. Visible and IR image of arc-jet test specimen.

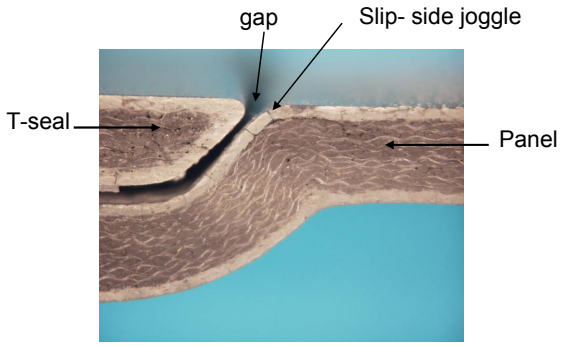


Figure 3. Close up photograph of cross-sectional view of test article in the vicinity of slip-side joggle.

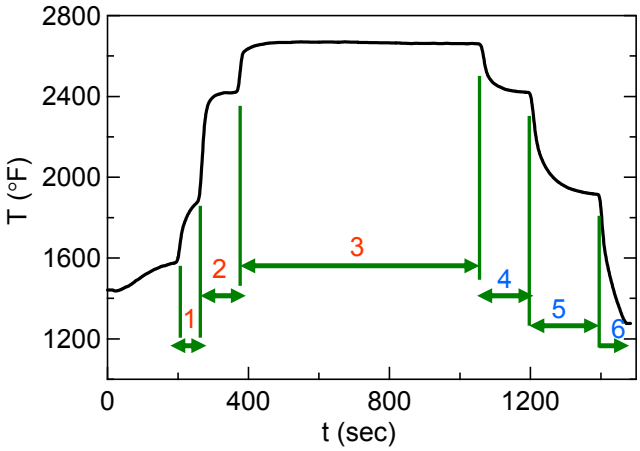


Figure 4. Nominal arc-jet surface temperatures measured using an optical pyrometer, and the various ramp up or down steps for RCC joggle tests.

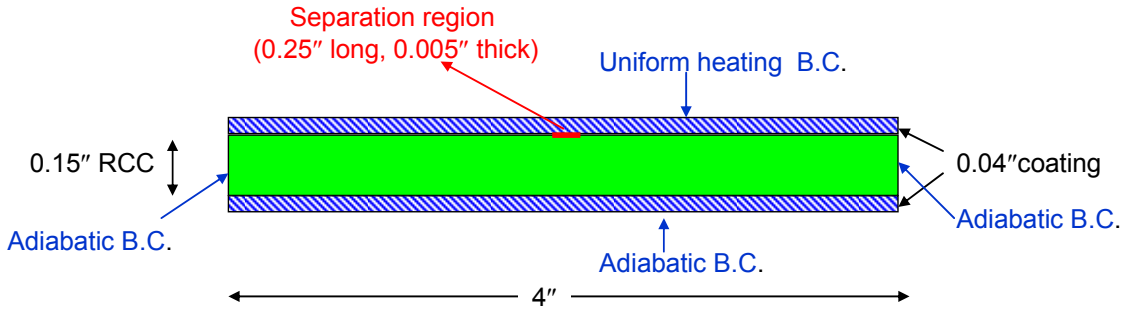


Figure 5. Geometry for simplified two-dimensional thermal analysis.

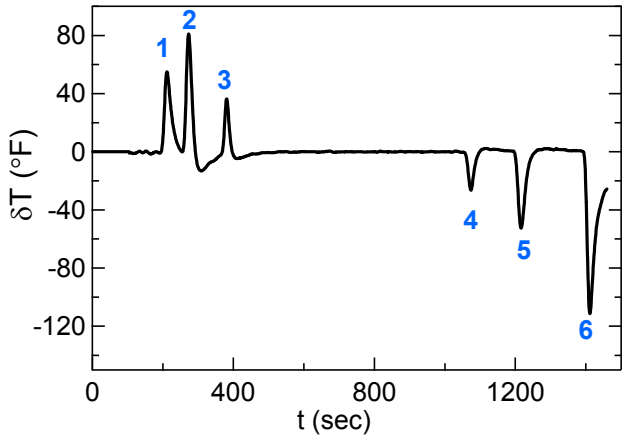


Figure 6. Predicted separation thermal signature for pre-existing subsurface material separation.

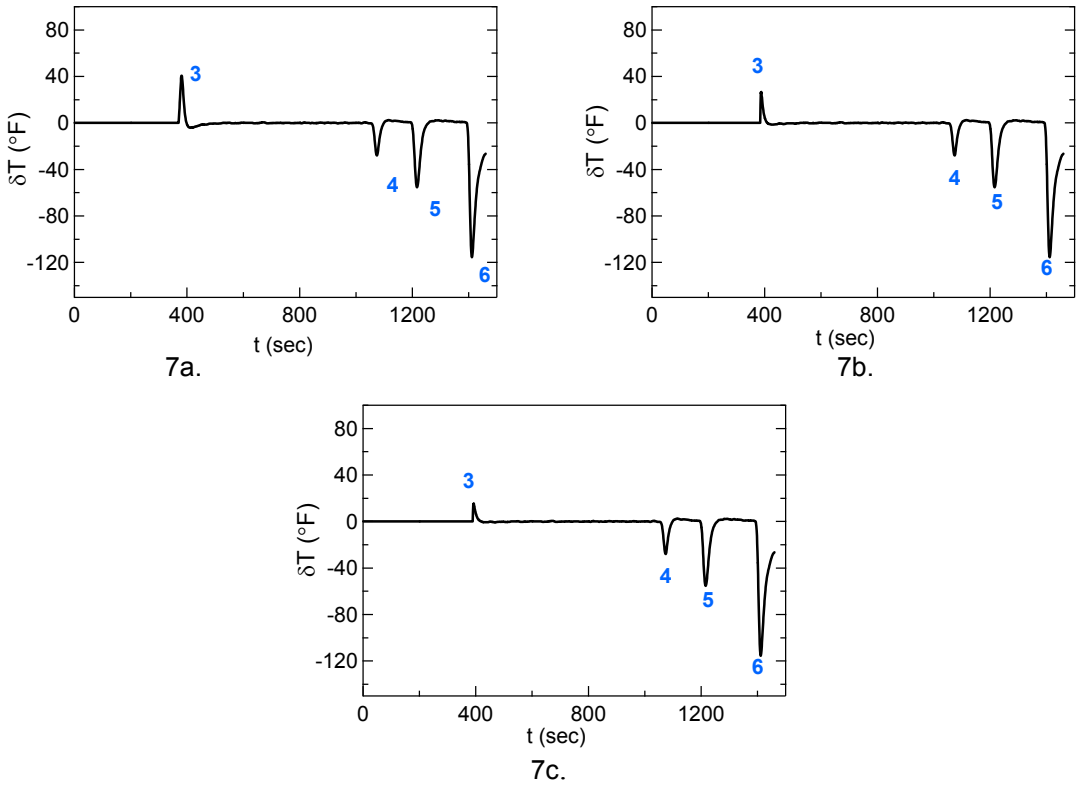


Figure 7. Variation of subsurface material separation thermal signature with separation initiation time: a) 371, b) 385, c) 390 sec.

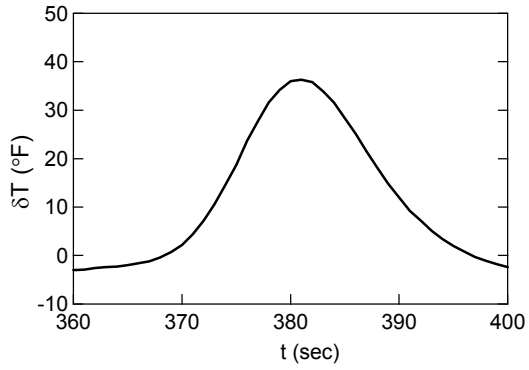


Figure 8. Detailed separation signature for SMS occurring at 371 sec.

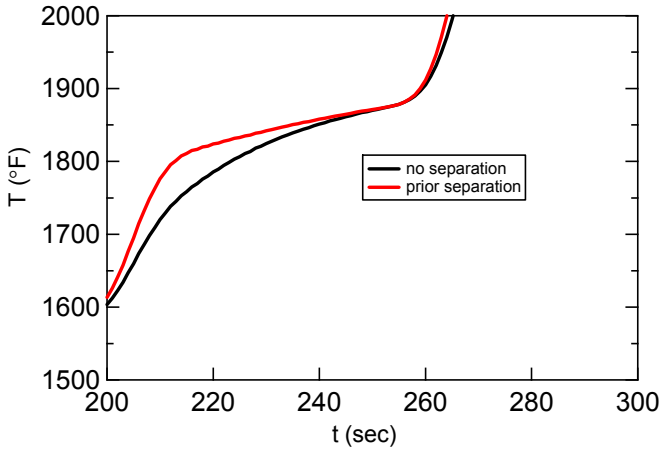


Figure 9. Predicted transient surface temperatures for arc-jet step 2 for models with and without prior subsurface material separation.

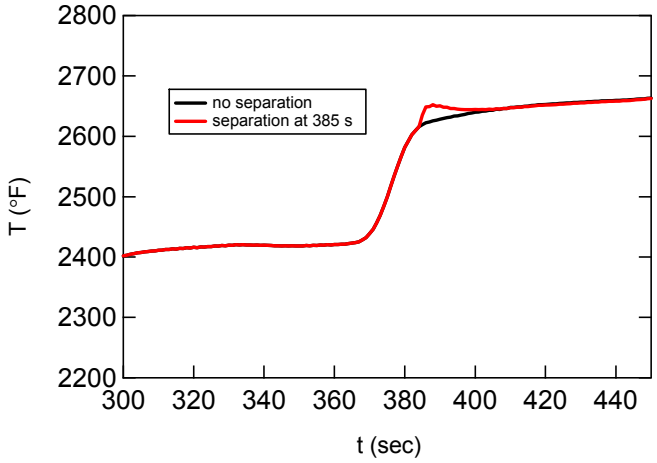


Figure 10. Predicted transient surface temperatures for arc-jet step 3 for model without subsurface material separation, and model with separation occurring at 385 sec.

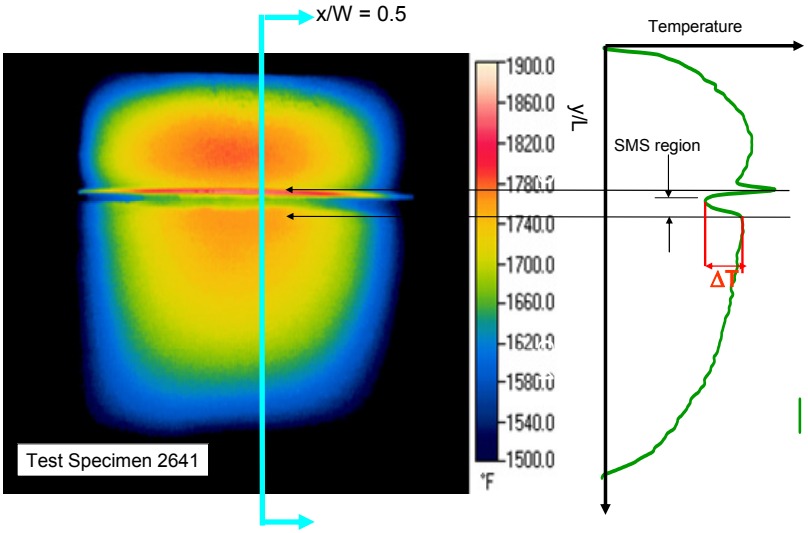


Figure 11. IR image of test specimen 2641 and the streamwise temperature distribution at mid-span at 1406.1 sec, showing nomenclature used for detecting subsurface material separation thermal signature.

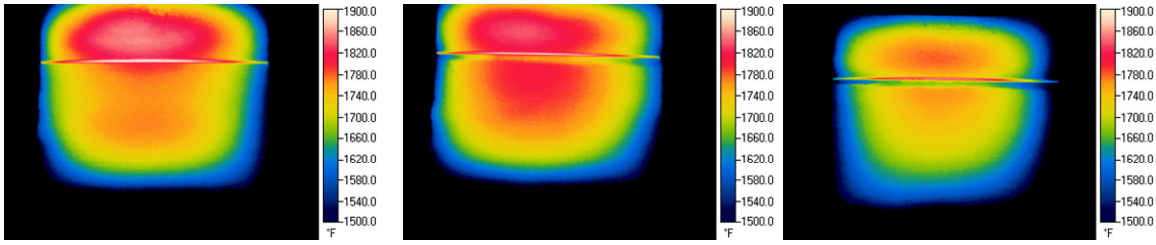

a) b) c)

Figure 12. IR images of three test specimens during arc-jet step 6 (ramp down from 2000°F) 6 sec after start of step: a) test specimen 2638 at 1406.1 sec, b) test specimen 2637 at 1406 sec, c) test specimen 2641 at 1406.1 sec.

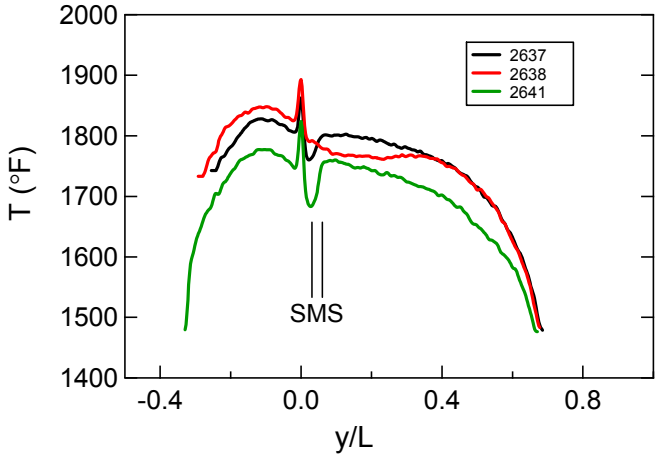


Figure 13. Streamwise temperature distributions at mid-span at 1406 sec for three test specimens during arc-jet step 6.

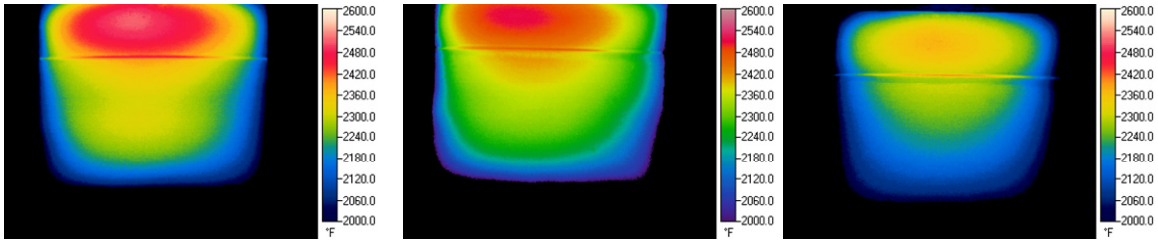


a) b) c)

Figure 14. IR images of three test specimens during arc-jet step 5 (ramp down to 2000°F) 14 sec after start of step: a) test specimen 2638 at 1214.2 sec, b) test specimen 2637 at 1214.2 sec, c) test specimen 2641 at 1214.7 sec.

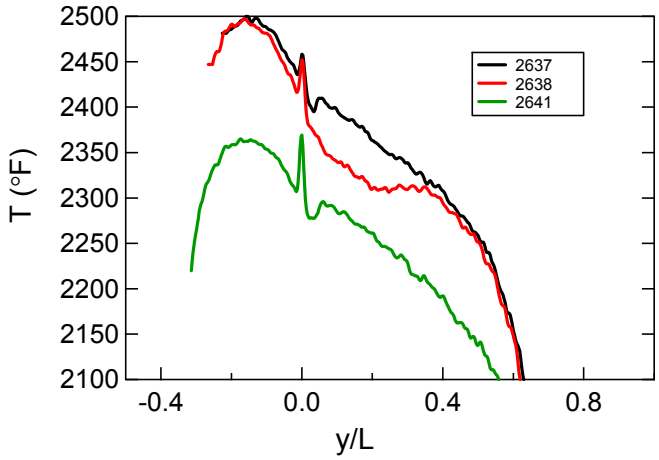


Figure 15. Streamwise temperature distributions at mid-span at 1214 sec for three test specimens during arc-jet step 5.

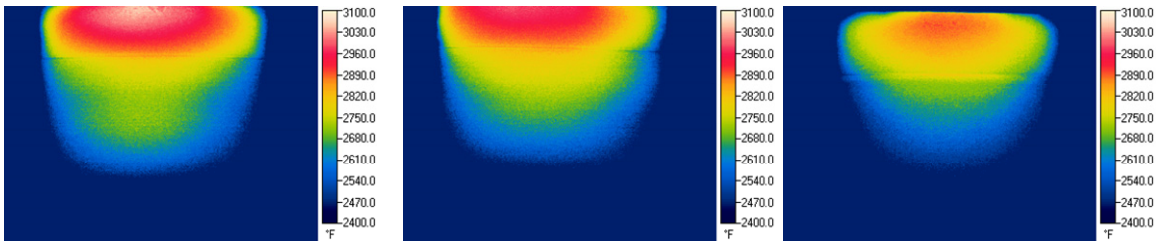


a) b) c)

Figure 16. IR images of three test specimens during arc-jet step 4 (ramp down to 2500°F) 12 sec after start of step: a) test specimen 2638 at 1071.3 sec, b) test specimen 2637 at 1072.7 sec, c) test specimen 2641 at 1072.9 sec.

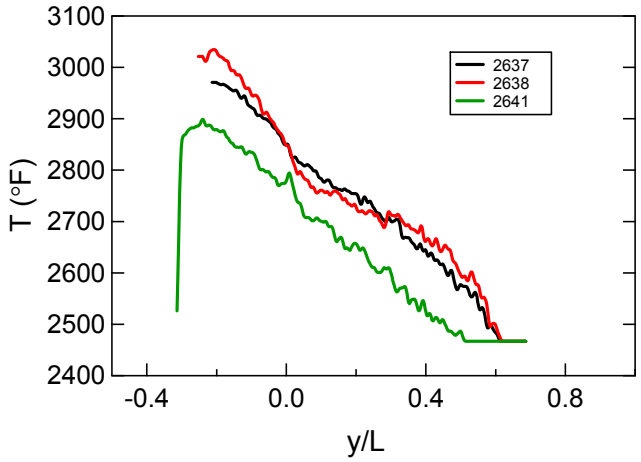


Figure 17. Streamwise temperature distributions at mid-span at 1072 sec for three test specimens during arc-jet step 4.

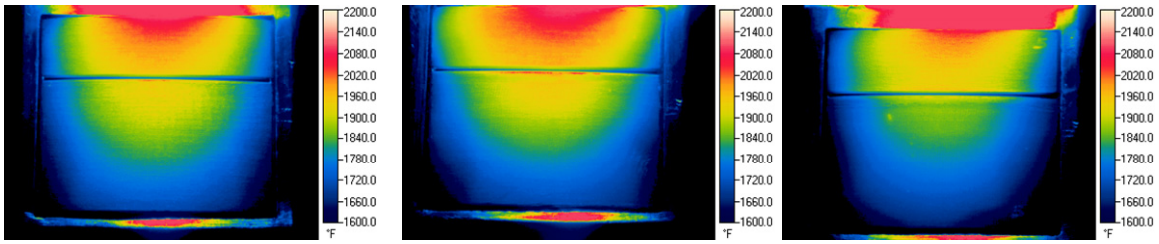


a) b) c)

Figure 18. IR images of three test specimens during arc-jet step 1 (ramp up to 2000°F) 10 sec after start of step: a) test specimen 2638 at 209.9 sec, b) test specimen 2637 at 209.9 sec, c) test specimen 2641 at 209.8 sec

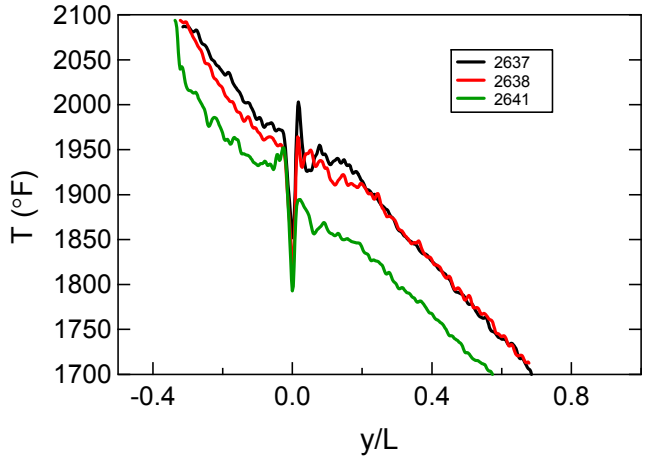


Figure 19. Streamwise temperature distributions at mid-span at 210 sec for three test specimens during arc-jet step 1.

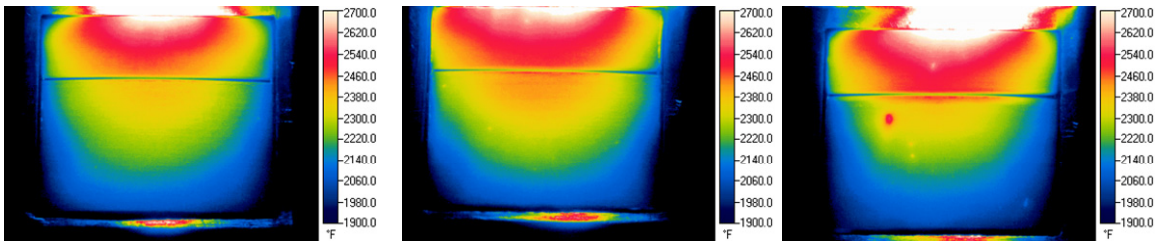


a) b) c)

Figure 20. IR images of three test specimens during arc-jet step 2 (ramp up to 2500°F) 10 sec after start of step: a) test specimen 2638 at 270 sec, b) test specimen 2637 at 270.9 sec, c) test specimen 2641 at 269.9 sec.

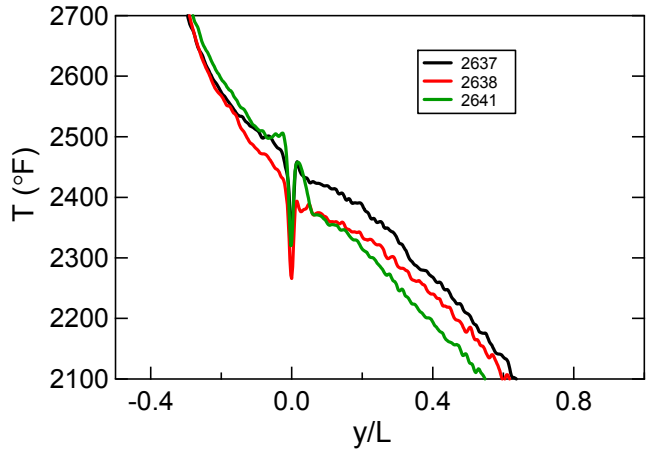


Figure 21. Streamwise temperature distributions at mid-span at 270 sec for three test specimens during arc-jet step 2.

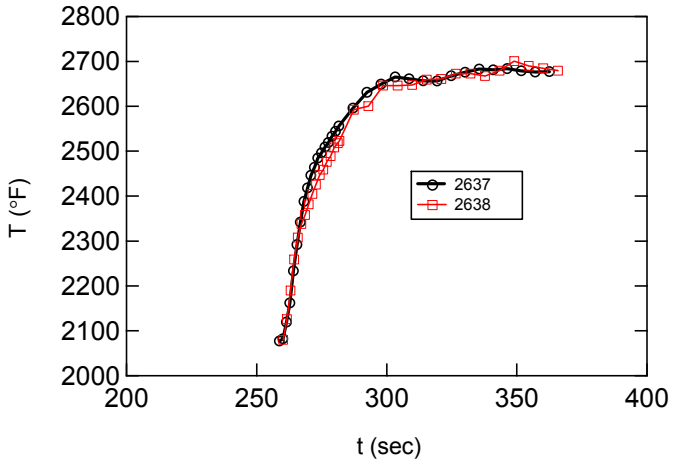


Fig 22. Transient surface temperatures in the joggle region during step 2 of arc-jet test (0.09-inch downstream of gap) for test specimens 2637 and 2638.

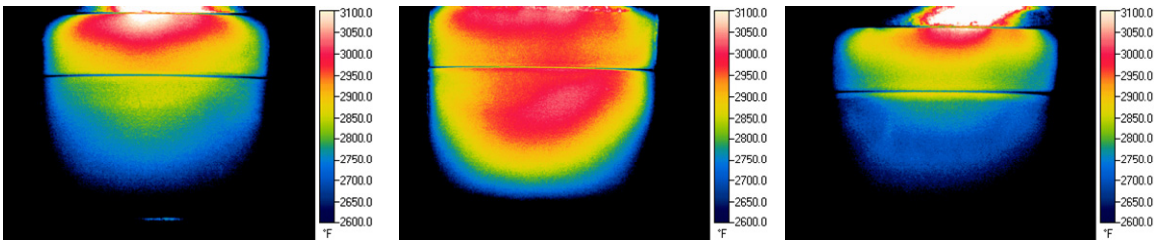


a) b) c)

Figure 23. IR images of three test specimens during arc-jet step 3 (ramp up to 2800°F) 11 sec after start of step: a) test specimen 2638 at 381.1 sec, b) test specimen 2637 at 381.1 sec, c) test specimen 2641 at 381 sec.

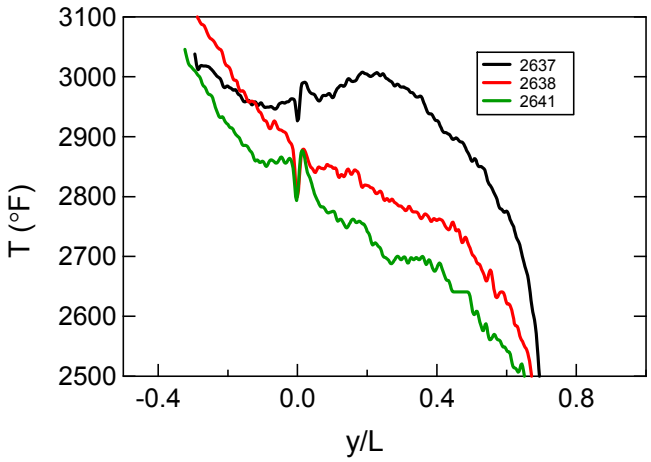


Figure 24. Streamwise temperature distributions at mid-span at 381 sec for three test specimens during arc-jet step 3.

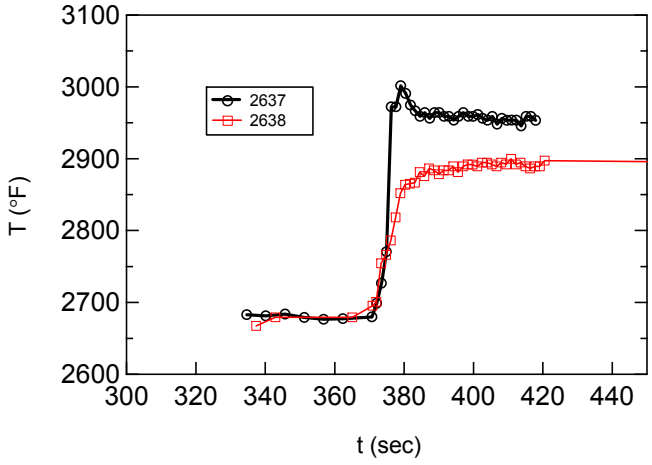


Figure 25. Transient surface temperatures in the joggle region during step 3 of arc-jet test (0.09-inch downstream of gap) for test specimens 2637 and 2638.